BIOCHEMISTRY
including biophysical chemistry & molecular biology
Article

Biochemistry **2010,** *49,* 5377–5389 5377
DOI: 10.1021/bi100538b

Role of Lys-12 in Catalysis by Triosephosphate Isomerase: A Two-Part Substrate Approach†

Maybelle K. Go, Astrid Koudelka, Tina L. Amyes, and John P. Richard*

Department of Chemistry, University at Buffalo, State University of New York, Buffalo, New York 14260-3000

Received April 9, 2010; Revised Manuscript Received May 17, 2010

ABSTRACT: We report that the K12G mutation in triosephosphate isomerase (TIM) from *Saccharomyces cerevisiae* results in (1) a ~50-fold increase in K_m for the substrate glyceraldehyde 3-phosphate (GAP) and a 60-fold increase in K_i for competitive inhibition by the intermediate analogue 2-phosphoglycolate, resulting from the loss of stabilizing ground state interactions between the alkylammonium side chain of Lys-12 and the ligand phosphodianion group; (2) a 12000-fold decrease in k_{cat} for isomerization of GAP, suggesting a tightening of interactions between the side chain of Lys-12 and the substrate on proceeding from the Michaelis complex to the transition state; and (3) a 6×10^5-fold decrease in k_{cat}/K_m, corresponding to a total 7.8 kcal/mol stabilization of the transition state by the cationic side chain of Lys-12. The yields of the four products of the K12G TIM-catalyzed isomerization of GAP in D_2O were quantified as dihydroxyacetone phosphate (DHAP) (27%), [1(*R*)-^{2}H]DHAP (23%), [2(*R*)-^{2}H]GAP (31%), and methylglyoxal (18%) from an *enzyme-catalyzed* elimination reaction. The K12G mutation has only a small effect on the relative yields of the three products of the transfer of a proton to the TIM-bound enediol(ate) intermediate in D_2O, but it strongly favors catalysis of the elimination reaction to give methylglyoxal. The K12G mutation also results in a ≥14-fold decrease in k_{cat}/K_m for isomerization of bound glycolaldehyde (GA), although the dominant observed product of the mutant enzyme-catalyzed reaction of [1-^{13}C]GA in D_2O is [1-^{13}C,2,2-di-^{2}H]GA from a nonspecific protein-catalyzed reaction. The observation that the K12G mutation results in a large decrease in k_{cat}/K_m for the reactions of both GAP and the neutral truncated substrate [1-^{13}C]GA provides evidence for a stabilizing interaction between the cationic side chain of Lys-12 and the negative charge that develops at the enolate-like oxygen in the transition state for deprotonation of the sugar substrate "piece".

Triosephosphate isomerase (TIM)[1] catalyzes the stereospecific, reversible, 1,2-hydrogen shift in dihydroxyacetone phosphate (DHAP) to give (*R*)-glyceraldehyde 3-phosphate (GAP) by a single-base (Glu-165) proton transfer mechanism through an enzyme-bound *cis*-enediol(ate) intermediate (Scheme 1) (*1*, *2*). The enzyme's low molecular mass (dimer, 26 kDa/subunit), its high cellular abundance (*3*), and the centrality of proton transfer at carbon in metabolic processes (*4*−*6*) have made TIM a prominent target for studies of the mechanism of enzyme action (*1*, *7*−*10*).

Deprotonation of the truncated neutral substrate (*R*)-glyceraldehyde by TIM is ~10^9-fold slower than the partly diffusion-controlled (*11*) turnover of the natural phosphorylated substrate GAP (*12*). We showed previously that more than 80% of the 4×10^{10}-fold enzymatic rate acceleration for carbon deprotonation of GAP is derived from the 12 kcal/mol "intrinsic phosphate binding energy" (*13*) of the small nonreacting phosphodianion group of the substrate (*12*, *14*). Similar intrinsic phosphate binding energies of 12 kcal/mol are observed for the decarboxylation reaction catalyzed by orotidine 5′-monophosphate decarboxylase (*15*) and the hydride transfer reaction catalyzed by glycerol-3-phosphate dehydrogenase (*16*).

Scheme 1

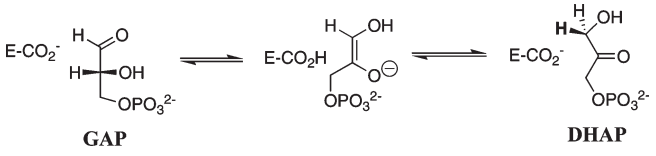

We want to understand the source of the large 12 kcal/mol intrinsic phosphate binding energy for TIM. X-ray crystallographic analyses of TIM in a complex with DHAP (*7*) or 2-phosphoglycolate (PGA) (*10*, *17*) reveal interactions between the ligand phosphodianion group and the backbone amide NH groups of Ser-211 in loop 7, Gly-232 and Gly-233 in loop 8, and Gly-171 in the flexible "phosphate gripper" loop 6 (*18*).[2] There should be little or no *enthalpic* advantage to stabilization of a TIM-bound ligand by hydrogen bonds between backbone amide NH groups

†This work was supported by Grant GM39754 from the National Institutes of Health.

*To whom correspondence should be addressed. Telephone: (716) 645-4232. Fax: (716) 645-6963. E-mail: jrichard@buffalo.edu.

[1]Abbreviations: TIM, triosephosphate isomerase; DHAP, dihydroxyacetone phosphate; GAP, (*R*)-glyceraldehyde 3-phosphate; PGA, 2-phosphoglycolate; GA, glycolaldehyde; GPDH, glycerol-3-phosphate dehydrogenase; BSA, bovine serum albumin; MES, 2-(*N*-morpholino)ethanesulfonic acid; CAPSO, 3-(cyclohexylamino)-2-hydroxy-1-propanesulfonic acid; NADH, nicotinamide adenine dinucleotide, reduced form; TEA, triethanolamine; MOPS, 3-(*N*-morpholino)propanesulfonic acid; *Pfu*, DNA polymerase from hyperthermophilic *Pyrococcus furiosus*; PCR, polymerase chain reaction; *Dpn*I, restriction endonuclease from *Diplococcus pneumoniae* G41; NMR, nuclear magnetic resonance; D,L-GAP, D,L-glyceraldehyde 3-phosphate; *d*-DHAP, [1(*R*)-^{2}H]-dihydroxyacetone phosphate; *d*-GAP, [2(*R*)-^{2}H]glyceraldehyde 3-phosphate; MG, methylglyoxal; PGH, 2-phosphoglycolohydroxamate.

[2]Unless noted otherwise, residues are numbered according to the sequence for the enzyme from yeast.

Published on Web 05/18/2010

and the ligand phosphodianion group, relative to its stabilization in aqueous solution by hydrogen bonding to water (*19*, *20*). However, there is probably a significant *entropic* advantage to formation of a network of four effectively intramolecular hydrogen bonds to a TIM-bound ligand relative to formation of four intermolecular hydrogen bonds in aqueous solution, because the latter is accompanied by the loss of translational and rotational entropy of four water molecules (*19*, *20*). Furthermore, hydrogen bonding to the backbone amide NH groups of Gly-232 and Gly-233 may be enhanced because these residues lie at the N-terminal end of a short α-helix that has its positive dipole directed toward the substrate phosphodianion group (*18*). We note, however, that it is difficult to examine by experiment the contribution of individual hydrogen bonds between substrate and backbone amide NH groups to the rate acceleration for TIM.

A major source of the intrinsic phosphate binding energy for TIM is the interaction between the substrate phosphodianion and the cationic alkylammonium side chain of Lys-12. The K12M mutant of yeast TIM was prepared in earlier work, but the effect of the mutation on the kinetic parameters could not be determined because the observed activity was due to contaminating wild-type TIM (*21*). This wild-type contaminant was presumed (*21*) to form as a result of rare errors in the translation of the methionine codon (AUG) to give the product of translation of the closely related lysine codon (AAG). The observation of respectable activities for both the K12R and K12H mutants of yeast TIM, along with a distinctive pH−rate profile for the K12H mutant, showed that a positively charged side chain at position 12 of TIM is required for the observation of robust enzymatic activity (*21*).

Electrostatic potential maps calculated from X-ray crystallographic data showed that the surface of the active site pocket for wild-type yeast TIM is cationic, while the corresponding surface for the K12M mutant is almost entirely anionic (*22*). These maps provided evidence that the cationic side chain of Lys-12 stabilizes the enzyme-bound substrate phosphodianion. However, it is not clear whether this interaction is expressed entirely at the Michaelis complex (K_m effect) or if it strengthens on proceeding to the transition state for deprotonation of the bound substrate (k_{cat} effect). We therefore aimed to characterize and quantify the effect of removal of the cationic side chain of Lys-12 on the activity of TIM, by substituting glycine for lysine at position 12. We have constructed the K12G mutant of yeast TIM by changing the native AAA lysine codon at position 12 to the GGC codon encoding glycine. This substitution effectively eliminates the possibility of contamination by the wild-type enzyme.

We report here the preparation of K12G mutant yeast TIM and the determination of the effect of this mutation on both the kinetic parameters and the product distribution for the turnover of the natural substrate GAP and of the truncated neutral substrate [1-^{13}C]glycolaldehyde ([1-^{13}C]GA). A comparison of the kinetic parameters for the wild-type and K12G TIM-catalyzed reactions of GAP shows that the alkylammonium side chain of Lys-12 stabilizes the transition state for isomerization of GAP by 7.8 kcal/mol. Approximately 30% of this interaction is expressed at the Michaelis complex with GAP, but ~70% (5.6 kcal/mol) is expressed specifically at the transition state for deprotonation of GAP (k_{cat} effect). We also observe a sizable effect of the K12G mutation on the kinetic parameters for isomerization of the truncated substrate [1-^{13}C]GA to give [2-^{13}C]GA, which provides strong evidence for a stabilizing interaction between the cationic side chain of Lys-12 and the negative charge that develops at the enolate-like oxygen in the transition state for deprotonation of this sugar substrate "piece".

MATERIALS AND METHODS

Materials. Glycerol-3-phosphate dehydrogenase from rabbit muscle (GPDH) and glycylglycine were from United States Biochemical. Bovine serum albumin (BSA) was from Roche. D,L-Glyceraldehyde 3-phosphate diethyl acetal (barium salt), dihydroxyacetone phosphate (lithium salt), 2-(*N*-morpholino)ethanesulfonic acid (MES), 3-(cyclohexylamino)-2-hydroxy-1-propanesulfonic acid (CAPSO), NADH (disodium salt), and Dowex 50WX4-200R were from Sigma. Triethanolamine hydrochloride (TEA·HCl) and imidazole were from Aldrich. 3-(*N*-Morpholino)-propanesulfonic acid (MOPS) and ethylamine hydrochloride were from Fluka. Sodium phosphite (dibasic, pentahydrate) was from Riedel-de Haën (Fluka). [1-^{13}C]Glycolaldehyde (99% enriched with ^{13}C at C-1, 0.09 M in water) was from Omicron Biochemicals. Deuterium oxide (99.9% D) and deuterium chloride [35% (w/w), 99.9% D] were from Cambridge Isotope Laboratories. DEAE Sepharose (fast flow) was from GE Healthcare. Water was obtained from a Milli-Q Academic purification system. Imidazole was recrystallized from benzene. All other commercially available chemicals were reagent grade or better and were used without further purification.

2-Phosphoglycolic acid was prepared according to a literature procedure (*23*). The barium salt of D-glyceraldehyde 3-phosphate diethyl acetal was prepared by J. Tait according to a literature procedure (*24*).

Preparation of Wild-Type and K12G Mutant Yeast TIM. The plasmid containing the gene for wild-type TIM from *Saccharomyces cerevisiae* (*25*) and *Escherichia coli* strain DF502 (strep^R, tpi$^-$, and his$^-$) whose DNA lacks the gene for TIM (*26*) were generous gifts from N. Sampson.

Site-directed mutagenesis of yeast TIM to introduce the K12G mutation was conducted using *Pfu* Ultra High Fidelity DNA polymerase following the Stratagene protocol. The starting plasmid DNA (30 ng) was placed into a PCR mixture containing 5 μL of 10× *Pfu* ultra buffer, 125 ng each of the forward and reverse mutagenesis primers, 5 μL of a 2 mM dNTP mixture, and 2.5 units of *Pfu* Ultra High Fidelity DNA polymerase in a final volume of 50 μL. The parameters for the PCR were as follows: 45 s at 95 °C followed by 17 cycles of 45 s at 95 °C, 1.5 min at 55 °C, and 10 min at 68 °C. The primer used to introduce the K12G mutation, in which the altered codon is underlined, was 5′-CT-TTC-TTT-GTC-GGT-GGT-AAC-TTT-GGC-TTA-AAC-GGT-TCC-AAA-CAA-TCC-3′. After completion of the PCR, 30 units of *Dpn*I was added to 30 μL of the reaction mixture followed by incubation for 1 h at 37 °C, to degrade the methylated template DNA. *E. coli* strain K802 was transformed with 1 μL of the *Dpn*I-digested PCR product. Several colonies containing possible mutants were picked, and the plasmid DNA was purified using the QIAprep Miniprep Kit from Qiagen. The presence of the gene for K12G mutant TIM was verified by sequencing at the Roswell Park Cancer Institute (Buffalo, NY).

E. coli strain DF502 was transformed with the plasmid containing the gene for wild-type or K12G mutant yeast TIM, and the proteins were expressed and purified according to published procedures, with ion exchange chromatography performed using DEAE Sepharose (*27*, *28*). The purity of the protein in the individual column fractions was determined by gel electrophoresis. Fractions containing the desired TIM at >95% purity were pooled and dialyzed against 20 mM TEA (pH 7.5).

Preparation of Solutions. The solution pH or pD was determined at 25 °C using an Orion model 720A pH meter equipped with a Radiometer pHC4006-9 combination electrode that was standardized at pH 7.00, and 4.00 or 10.00 at 25 °C. Values of pD were obtained by adding 0.40 to the observed reading of the pH meter (*29*).

The volume of [1-^{13}C]glycolaldehyde (1 mL of a 90 mM solution in H_2O) was reduced to ~100 μL by rotary evaporation. Five milliliters of D_2O was added, and the volume was again reduced to ~100 μL by rotary evaporation. This procedure was repeated twice more, and 900 μL of D_2O was added to the final solution to give a volume of ~1 mL. The stock solution of [1-^{13}C]GA in D_2O was stored at room temperature to minimize the content of glycolaldehyde dimer (*30*). The concentration of [1-^{13}C]GA in the stock solution was determined by ^{1}H NMR spectroscopy, as described previously (*28*, *30*, *31*).

Solutions of GAP in D_2O and of D,L-glyceraldehyde 3-phosphate (D,L-GAP) in H_2O were prepared by hydrolysis of the corresponding diethyl acetals, as described previously (*28*, *32*). The resulting solutions were stored at −20 °C. These solutions were adjusted to the appropriate pD or pH using 1 M NaOD or 1 M NaOH before use, after which they were again stored at −20 °C. The stock solution of PGA was prepared in D_2O and was adjusted to pD 6.9 with 1 M NaOD before use. The concentration of PGA in the stock solution was determined by ^{1}H NMR as follows. An aliquot (50 μL) of the stock solution of PGA was added to 700 μL of 30 mM imidazole buffer (pD 7.0, 20% free base). Comparison of the integrated areas of the signals due to the C-4 and C-5 protons of imidazole and the C-2 protons of PGA gave a concentration of PGA in the stock solution of 42 mM.

Buffered solutions of TEA, MES, MOPS, glycylglycine, and carbonate in H_2O were prepared by neutralization of the acidic form with sufficient 1 M NaOH to give the desired pH. Buffered solutions of acetate and CAPSO in H_2O were prepared via addition of sufficient 1 M HCl to the sodium salt to yield the desired pH.

Before the preparation of solutions in D_2O, the bulk of the water of crystallization of $Na_2HPO_3 \cdot 5H_2O$ was removed by in vacuo drying as described previously (*30*). The acidic protons of ethylamine hydrochloride were exchanged for deuterium by repeated dissolution in D_2O followed by removal of the solvent under reduced pressure and in vacuo drying. The stock solution of $EtND_3^+Cl^-$ in D_2O was adjusted to pD 6.7 using 1 M NaOD. Buffered solutions of imidazole and phosphite in D_2O were prepared by dissolving the basic form, and where appropriate NaCl, followed by the addition of a measured amount of a stock solution of DCl to give the desired buffer ratio.

Enzyme Assays. All enzyme assays were conducted at 25 °C. One unit is the amount of enzyme that converts 1 μmol of substrate to product in 1 min under the specified conditions.

Changes in the concentration of NADH were calculated using an extinction coefficient of 6220 M^{-1} cm^{-1} at 340 nm. We dialyzed GPDH at 4 °C against 20 mM TEA (pH 7.5) and assayed GPDH by monitoring the oxidation of NADH by DHAP at 340 nm, as described previously (*28*). Dilute solutions of TIM were stabilized by the inclusion of 0.01% (0.1 mg/mL) BSA. The subunit concentration of wild-type or K12G yeast TIM in stock solutions was determined from the absorbance at 280 nm using an extinction coefficient of 2.55×10^4 M^{-1} cm^{-1} that was calculated using the ProtParam tool available on the ExPASy server (*33*, *34*). The concentration of GAP in stock solutions of GAP in D_2O or of D,L-GAP in H_2O was determined from the amount of NADH consumed during quantitative TIM-catalyzed isomerization of GAP to form DHAP that was coupled to the oxidation of NADH using GPDH.

The activities of wild-type and K12G mutant yeast TIM were determined by coupling the isomerization of GAP to form DHAP to the oxidation of NADH using GPDH (*35*). The standard assay mixture (1.0 mL) contained 30 mM TEA (pH 7.5), 0.2 mM NADH, 5 mM D,L-GAP (2.5 mM GAP), and ~1 unit of GPDH at an ionic strength of 0.10 (NaCl). A low background velocity v_o that is due mainly to the isomerization of GAP catalyzed by TIM that was present as an impurity in the commercial preparation of GPDH was determined over a period of 2−4 min. An aliquot of wild-type or K12G TIM was then added, and the total initial velocity v_{obs} was determined by monitoring the reaction for an additional 5−10 min. The initial velocity of the TIM-catalyzed reaction (v_i) was then calculated with the relationship $v_i = v_{obs} - v_o$, where v_o generally represented ≤2% of v_{obs}.

Values of K_i for competitive inhibition of wild-type and K12G mutant yeast TIM by PGA at pH 7.5 (30 mM TEA), 25 °C, and an ionic strength of 0.10 (NaCl) were determined using several concentrations of PGA up to 130 μM for wild-type TIM or 2.1 mM for K12G mutant TIM.

pH−Rate Profile for Turnover of GAP by K12G TIM. The pH dependence of k_{cat}/K_m for isomerization of GAP catalyzed by K12G mutant yeast TIM at 25 °C was determined using the following buffers: acetate for pH 5.1, MES for pH 5.6 and 6.3, MOPS for pH 7.1, TEA for pH 7.5, glycylglycine for pH 8.3, CAPSO for pH 8.9, and carbonate for pH 9.9. The standard assay mixture (1.0 mL) contained 30 mM buffer, 0.2 mM NADH, 0.8−6 mM D,L-GAP (0.4−3 mM GAP), and ~1 unit of GPDH. The relative specific activity of the coupling enzyme GPDH was determined at each pH, and the amount used was adjusted so that the velocity of consumption of NADH was independent of the concentration of the coupling enzyme (*35*).

^{1}H NMR Analyses. ^{1}H NMR spectra at 500 MHz were recorded in D_2O at 25 °C using a Varian Unity Inova 500 spectrometer that was shimmed to give a line width of ≤0.7 Hz for each peak of the doublet due to the C-1 proton of GAP hydrate, or ≤0.5 Hz for the downfield peaks of the double triplet due to the C-1 proton of [1-^{13}C]GA hydrate. Spectra (16−64 transients) were recorded using a sweep width of 6000 Hz, a pulse angle of 90°, and an acquisition time of 4−6 s, with zero-filling of the data to 128 K. To ensure accurate integrals for the protons of interest, a relaxation delay between pulses of 120 s ($>8T_1$) was used. Baselines were subjected to a first-order drift correction before determination of integrated peak areas. Chemical shifts are reported relative to HOD at 4.67 ppm.

K12G TIM-Catalyzed Reaction of GAP in D_2O Monitored by ^{1}H NMR. K12G TIM was exhaustively dialyzed at 4 °C against 10 mM imidazole (pD 7.9, 70% free base) in D_2O at an ionic strength of 0.10 (NaCl). The reaction of GAP (10 mM) in the presence of K12G TIM in D_2O at pD 7.9 (10 mM imidazole), 25 °C, and an ionic strength of 0.15 (NaCl) was monitored by ^{1}H NMR spectroscopy, as described previously (*32*). The fraction of the remaining substrate GAP (f_{GAP}) and the fraction of GAP converted to products DHAP (f_{DHAP}), *d*-DHAP ($f_{d\text{-DHAP}}$), *d*-GAP ($f_{d\text{-GAP}}$), and methylglyoxal (f_{MG}) at time *t* were determined from the integrated areas of the relevant ^{1}H NMR signals (normalized using the signal due to the C-4 and C-5 protons of imidazole as an internal standard), as described previously (*32*). A control experiment was conducted to monitor the rate of the nonenzymatic elimination reaction of GAP (10 mM) to give

methylglyoxal (*14*) in D_2O at pD 7.9 (10 mM imidazole), 25 °C, and an ionic strength of 0.15 (NaCl).

K12G TIM-Catalyzed Reactions of [1-^{13}C]GA in D_2O Monitored by ^{1}H NMR. K12G TIM was exhaustively dialyzed at 4 °C against 30 mM imidazole (pD 7.0, 20% free base) in D_2O at an ionic strength of 0.10 (NaCl) for reactions in the absence of phosphite and/or $EtND_3^+$, or at an ionic strength of 0.024 for reactions in their presence.

The K12G TIM-catalyzed reaction of [1-^{13}C]GA in D_2O at pD 7.0 (reaction 1) was initiated by addition of 650 μL of enzyme (~13 mg/mL) to 350 μL of a solution containing [1-^{13}C]GA and NaCl to give final concentrations of 20 mM [1-^{13}C]GA, 20 mM imidazole, and 240 μM K12G TIM in D_2O at pD 7.0 and an ionic strength of 0.10 (NaCl). The K12G TIM-catalyzed reaction of [1-^{13}C]GA in D_2O at pD 7.0 in the presence of 100 mM $EtND_3^+$ (reaction 2) was initiated by addition of 650 μL of enzyme (~13 mg/mL) to 350 μL of a solution containing [1-^{13}C]GA and $EtND_3^+$ to give final concentrations of 20 mM [1-^{13}C]GA, 20 mM imidazole, 100 mM $EtND_3^+$, and 310 μM K12G TIM in D_2O at pD 7.0 and an ionic strength of 0.12. The K12G TIM-catalyzed reaction of [1-^{13}C]GA in D_2O at pD 7.0 in the presence of 50 mM $EtND_3^+$ and 10 mM phosphite dianion (20 mM total phosphite) (reaction 3) was initiated by addition of 600 μL of enzyme (~9 mg/mL) to 250 μL of a solution containing [1-^{13}C]GA, phosphite buffer (50% free base), and $EtND_3^+$ to give final concentrations of 20 mM [1-^{13}C]GA, 20 mM imidazole, 50 mM $EtND_3^+$, 10 mM phosphite dianion (20 mM total phosphite), and 290 μM K12G TIM in D_2O at pD 7.0 and an ionic strength of 0.12.

In each case, 750 μL of the reaction mixture was transferred to an NMR tube and ^{1}H NMR spectra (32 transients) at 25 °C were recorded over a period of 4−7 days. The remaining portion of the reaction mixture was incubated at 25 °C, and the activity of K12G TIM was monitored by a periodic standard assay (see above). For reaction 1, there was an ~20% drop in the activity of K12G TIM over 78 h at 25 °C. For reactions 2 and 3, there was an ~40% drop in the activity of K12G TIM over 7 days at 25 °C.

The fraction of the remaining substrate [1-^{13}C]GA (f_S) and the fraction of [1-^{13}C]GA converted to identifiable products [1-^{13}C,2-^{2}H]GA and [1-^{13}C,2,2-di-^{2}H$_2$]GA were determined from the integrated areas of the relevant ^{1}H NMR signals (normalized using the signal due to the C-4 and C-5 protons of imidazole as an internal standard), as described previously (*28*).

Observed first-order rate constants, k_{obs}, for the disappearance of [1-^{13}C]GA were determined from the slopes of linear semilogarithmic plots of reaction progress versus time according to eq 1

$$\ln f_S = -k_{obs}t \quad (1)$$

Observed second-order rate constants for the total protein-catalyzed reactions of [1-^{13}C]GA were calculated using eq 2

$$\left(\frac{k_{cat}}{K_m}\right)_{obs} = \frac{k_{obs}}{f_{car}[E]} \quad (2)$$

where f_{car} (0.061) is the fraction of GA present in the reactive carbonyl form (*30*, *31*) and [E] is the concentration of K12G TIM.

RESULTS

K12G TIM-Catalyzed Reaction of GAP in D_2O. The disappearance of the substrate and the appearance of the products of the nonenzymatic and K12G TIM-catalyzed reactions of GAP in D_2O were monitored by ^{1}H NMR spectroscopy, as described previously (*32*). Figure 1A shows the time course for the disappearance of GAP (10 mM) catalyzed by 85 μM K12G TIM in D_2O at pD 7.9 (10 mM imidazole), 25 °C, and an ionic strength of 0.15 (NaCl). The solid line shows the nonlinear least-squares fit of the experimental data to a single exponential which gave a k_{obs} of 3.6×10^{-4} s^{-1} as the observed rate constant for the disappearance of GAP (Table 1). Figure 1B shows the time dependence of the observed fractional yields of the four products of this reaction, $(f_P)_{obs}$ (P = DHAP, *d*-DHAP, *d*-GAP, or MG). These fractional yields were calculated from the fraction of the particular product P (see Materials and Methods) and the sum of the fractions of all the products of both the enzymatic and nonenzymatic reactions of GAP using eq 3 (Scheme 2). There is no significant change in $(f_P)_{obs}$ for DHAP with time, but the changes with time in the observed fractional yields of *d*-DHAP (increasing) and *d*-GAP (decreasing) result from

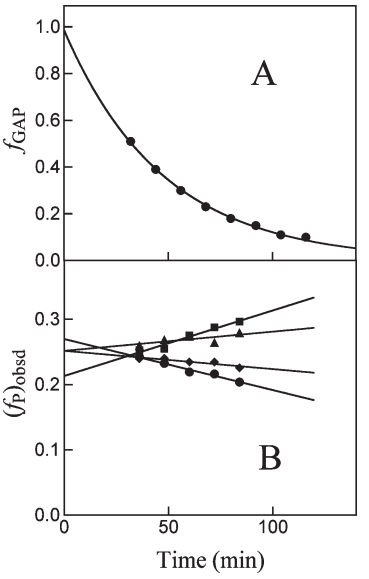

FIGURE 1: Data for the reaction of GAP (10 mM) in the presence of 85 μM K12G TIM in D_2O at pD 7.9 (10 mM imidazole), 25 °C, and an ionic strength of 0.15 (NaCl) monitored by ^{1}H NMR spectroscopy. (A) Time course for the first-order disappearance of the substrate GAP. (B) Dependence of the observed fractional yields of the products on time. Extrapolation of these data to zero time (—) gave the initial fractional yields of the products of the enzyme-catalyzed and nonenzymatic reactions of GAP, $(f_P)_o$ or $(f_{MG})_{tot} = (f_{MG})_N + (f_{MG})_E$, reported in Table 1: (◆) methylglyoxal, (■) *d*-DHAP, (▲) DHAP, and (●) *d*-GAP.

Scheme 2

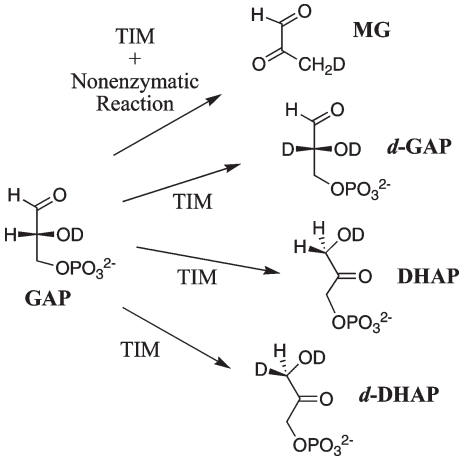

Table 1: Fractional Product Yields for the Reaction of (*R*)-Glyceraldehyde 3-Phosphate in the Presence of K12G Mutant Yeast Triosephosphate Isomerase in D_2O[a]

[K12G TIM] (μM)	k_{obs} (s^{-1})[b]		MG $(f_{MG})_{tot}$[c]	MG $(f_{MG})_N$[d]	MG $(f_{MG})_E$[e]	*d*-GAP $(f_P)_o$[f]	DHAP $(f_P)_o$[f]	*d*-DHAP $(f_P)_o$[f]
85	3.6×10^{-4}		0.25	0.05	0.20	0.27	0.25	0.21
		f_E[g]			0.21	0.28	0.26	0.22
		$(f_E)_{PT}$[h]				0.35	0.33	0.28
12	8.2×10^{-5}		0.34	0.21	0.13	0.26	0.22	0.19
		f_E[g]			0.16	0.33	0.28	0.24
		$(f_E)_{PT}$[h]				0.40	0.33	0.29
average values		f_E[g]			0.18 ± 0.02	0.31 ± 0.03	0.27 ± 0.01	0.23 ± 0.01
		$(f_E)_{PT}$[h]				0.38 (0.21)[i]	0.33 (0.49)[i]	0.29 (0.31)[i]

[a]Product distributions for the reaction of GAP (10 mM) at pD 7.9 (10 mM imidazole), 25 °C, and an ionic strength of 0.15 (NaCl) were determined by ^{1}H NMR spectroscopy as described previously (*32*). [b]Observed first-order rate constant for the disappearance of GAP in the presence of the indicated concentration of K12G TIM. [c]Total initial fractional yield of methylglyoxal determined by extrapolation of $(f_P)_{obs}$ to zero time (intercept in Figure 1B). [d]Initial fractional yield of methylglyoxal from the competing nonenzymatic reaction of GAP, calculated using eq 4. [e]Initial fractional yield of methylglyoxal from the enzymatic reaction of GAP, calculated using eq 5. [f]Initial fractional product yields determined by extrapolation of $(f_P)_{obs}$ to zero time (intercepts in Figure 1B). [g]Normalized fractional yields of the products of the enzymatic reaction of GAP, calculated using eq 9. [h]Normalized fractional yields of the three products of the transfer of a proton to the enzyme-bound enediolate intermediate, calculated using eq 10. [i]Data for the wild-type enzyme from chicken muscle taken from previous work (*32*).

enzyme-catalyzed isomerization of *d*-GAP to give the thermodynamically favored product *d*-DHAP (*32*). Table 1 reports the initial fractional product yields, $(f_P)_o$, for DHAP, *d*-DHAP, and *d*-GAP, or $(f_{MG})_{tot}$ for MG, that were determined by extrapolation of the observed product yields $(f_P)_{obs}$ to zero time (intercepts in Figure 1B).

$$(f_P)_{obs} = \frac{f_P}{f_{DHAP} + f_{d\text{-DHAP}} + f_{d\text{-GAP}} + f_{MG}} \quad (3)$$

$$(f_{MG})_N = \frac{k_N}{k_{obs}} \quad (4)$$

$$(f_{MG})_E = (f_{MG})_{tot} - (f_{MG})_N \quad (5)$$

In a control experiment, the nonenzymatic elimination reaction of GAP (10 mM) to form methylglyoxal (*14*) in D_2O at pD 7.9 (10 mM imidazole), 25 °C, and an ionic strength of 0.15 (NaCl) was monitored by ^{1}H NMR spectroscopy (*32*). The fit of the data to a single exponential gave an observed first-order rate constant for the disappearance of GAP (k_N) of 1.7×10^{-5} s^{-1}. This was combined with a k_{obs} of 3.6×10^{-4} s^{-1} for the reaction of GAP in the presence of 85 μM K12G TIM, according to eq 4, to give the calculated fractional yield of methylglyoxal from the nonenzymatic elimination reaction in this experiment [$(f_{MG})_N$ = 0.05 (Table 1)]. The total initial fractional yield of methylglyoxal [$(f_{MG})_{tot}$] of 0.25 (Table 1) is 5-fold larger than $(f_{MG})_N$ because, unlike wild-type TIM, K12G TIM also catalyzes the elimination reaction of GAP to give methylglyoxal. The initial fractional yield of methylglyoxal from the K12G TIM-catalyzed reaction [$(f_{MG})_E$] of 0.20 (Table 1) was calculated using eq 5.

K12G TIM-Catalyzed Reaction of [1-^{13}C]GA in D_2O. Figure 2 shows semilogarithmic plots according to eq 1 of the time course for the disappearance of [1-^{13}C]GA in D_2O at pD 7.0 (20 mM imidazole) and 25 °C, monitored by ^{1}H NMR spectroscopy (*28*), in the presence of K12G TIM, K12G TIM and 100 mM $EtND_3^+$, or K12G TIM, 50 mM $EtND_3^+$, and 10 mM phosphite dianion (20 mM total phosphite). Table 2 gives the observed first-order rate constants for these reactions that were calculated from the slopes of these linear correlations that covered one to two half-times.

Figure 3 shows portions of the ^{1}H NMR spectrum at 500 MHz of the reaction mixture obtained from the reaction of [1-^{13}C]GA

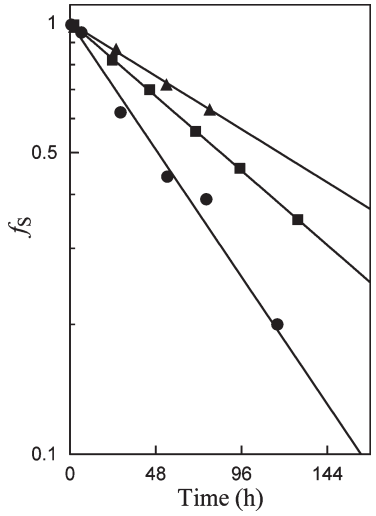

FIGURE 2: Semilogarithmic plots of the fraction of the remaining substrate vs time for the reaction of [1-^{13}C]glycolaldehyde in the presence of K12G TIM in D_2O at pD 7.0 (20 mM imidazole) and 25 °C. The observed rate constants were determined from the slopes according to eq 1: (▲) 240 μM K12G TIM at an ionic strength of 0.10, (■) 310 μM K12G TIM and 100 mM $EtND_3^+$ at an ionic strength of 0.12, and (●) 290 μM K12G TIM, 50 mM $EtND_3^+$, and 10 mM HPO_3^{2-} at an ionic strength of 0.12.

for 78 h in the presence of 240 μM K12G TIM in D_2O at pD 7.0 and 25 °C. Under our reaction conditions, glycolaldehyde exists as 93.9% hydrate and 6.1% free carbonyl form (*30*, *31*), and the following chemical shifts refer to the hydrates of the isotopomers shown in Chart 1. The signal due to the C-1 proton of [1-^{13}C]GA appears as a double triplet at 4.945 ppm ($^1J_{HC}$ = 163 Hz; $^3J_{HH}$ = 5 Hz) (Figure 3B). The signal due to the C-1 proton of [1-^{13}C,2,2-di-^{2}H]GA appears as a broad doublet ($^1J_{HC}$ = 163 Hz) at 4.930 ppm that is shifted 0.015 ppm upfield from the double triplet due to the C-1 proton of [1-^{13}C]GA as a result of the two β-deuteriums (Figure 3B). The signal due to the C-2 protons of [1-^{13}C]GA appears as a double doublet at 3.410 ppm ($^2J_{HC}$ = 3 Hz; $^3J_{HH}$ = 5 Hz) (Figure 3A). The signals due to the C-2 protons of [2-^{13}C]GA and [1,2-di-^{13}C]GA, present initially at 0.8 and 0.9%, respectively, in our commercial [1-^{13}C]GA, appear at 3.410 ppm as a double doublet ($^1J_{HC}$ = 142 Hz; $^3J_{HH}$ = 5 Hz) and a double double

Table 2: Rate and Product Data for the Reactions of [1-^{13}C]GA in the Presence of K12G Mutant Yeast Triosephosphate Isomerase and the Potential Activators $EtND_3^+$ and Phosphite Dianion in D_2O[a]

[K12G TIM] (μM)	activator	k_{obs}[b] (s^{-1})	$(k_{cat}/K_m)_{obs}$[c] (M^{-1} s^{-1})	$(k_{cat}/K_m)_{iso}$[d] (M^{-1} s^{-1})	fractional product yield			
					[2-^{13}C]GA	[1-^{13}C,2-^{2}H]GA	[1-^{13}C,2,2-di-^{2}H$_2$]GA	total[e]
240	none[f]	1.6×10^{-6}	0.11	$\leq 7 \times 10^{-4}$	$\leq$0.006[g]	small	0.56	0.56
310	100 mM $EtND_3^{+}$[h]	2.3×10^{-6}	0.12		none detected	0.10	0.20	0.30
290	50 mM $EtND_3^+$ and 10 mM HPO_3^{2-}[h]	3.8×10^{-6}	0.22		none detected	0.14	0.19	0.32

[a]Product distributions for the reaction of [1-^{13}C]GA (20 mM) at pD 7.0 (20 mM imidazole) and 25 °C were determined by ^{1}H NMR spectroscopy as described previously (*28*). [b]Observed first-order rate constant for the disappearance of [1-^{13}C]GA. [c]Total observed second-order rate constant for the specific and nonspecific protein-catalyzed reactions. [d]Second-order rate constant for the specific K12G TIM-catalyzed isomerization of [1-^{13}C]GA to give [2-^{13}C]GA, calculated as the product of the $(k_{cat}/K_m)_{obs}$ (0.11 M^{-1} s^{-1}) and 0.006 as the upper limit on the fractional yield of [2-^{13}C]GA. [e]Total fractional yield of the identifiable products. [f]At an ionic strength of 0.10 (NaCl). [g]Upper limit on the fractional yield of [2-^{13}C]GA (see the text). [h]At an ionic strength of 0.12 (NaCl).

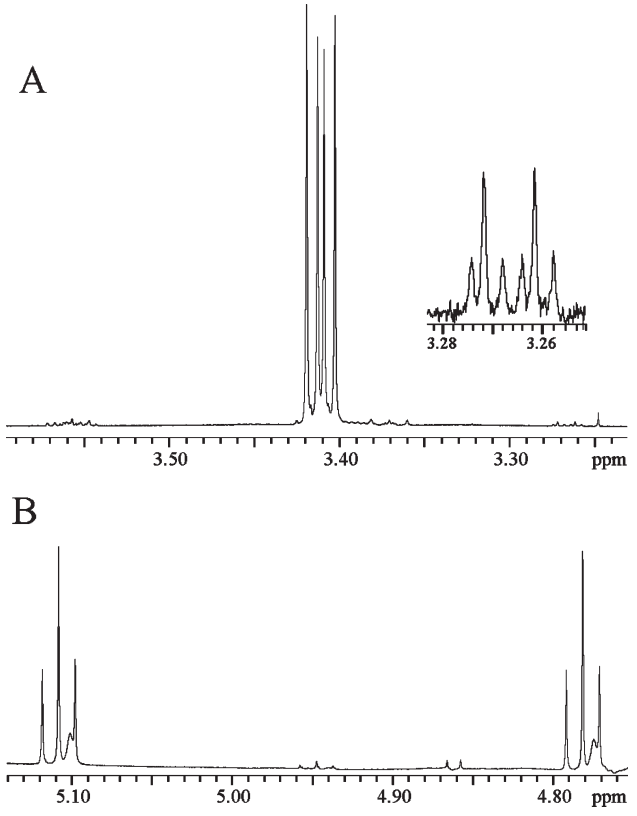

FIGURE 3: Portions of the ^{1}H NMR spectrum at 500 MHz of the reaction mixture obtained from the reaction of [1-^{13}C]GA (20 mM) for 78 h in the presence of 240 μM K12G TIM in D_2O at pD 7.0, 25 °C, and an ionic strength of 0.10 (NaCl). (A) Spectrum in the region of the C-2 hydron(s) of the isotopomers of GA. (B) Spectrum in the region of the C-1 hydron of the isotopomers of GA.

doublet ($^1J_{HC}$ = 142 Hz; $^2J_{HC}$ = 3 Hz; $^3J_{HH}$ = 5 Hz), respectively. Figure 3A (inset) shows the upfield peaks of these signals; the corresponding downfield peaks appear along with other small peaks for unidentified reaction products.

We observe that the major identifiable product of the reaction of [1-^{13}C]GA in the presence of K12G mutant TIM in D_2O is the doubly deuteriated isotopomer [1-^{13}C,2,2-di-^{2}H]GA which is formed in a *nonspecific* reaction occurring outside the active site (*28*). The fractional yield of this product [f_P = 0.56 (Table 2)] was calculated from the normalized peak area for its C-1 proton, A_P, and the difference in the normalized peak area for the C-1 proton of the substrate [1-^{13}C]GA at time zero, $(A_S)_o$, and at time t, A_S, according to eq 6. The signal due to the C-2 proton of the

Chart 1

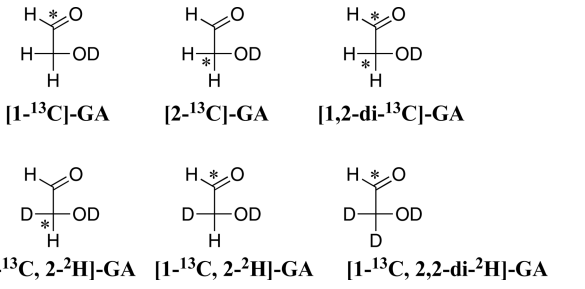

product of isomerization with deuterium exchange, [2-^{13}C,2-^{2}H]GA, would appear as a double double triplet at 3.389 ppm ($^1J_{HC}$ = 142 Hz; $^3J_{HH}$ = 5 Hz; $^2J_{HD} \approx$ 2 Hz) shifted 0.021 ppm upfield of the double doublet due to the C-2 protons of [2-^{13}C]GA as a result of the α-deuterium (*28*). However, this signal was not observed in the spectrum shown in Figure 3A.

$$f_P = \frac{A_P}{(A_S)_o - A_S} \quad (6)$$

During the reaction of [1-^{13}C]GA catalyzed by wild-type TIM in D_2O, we observed that enzyme-catalyzed isomerization of the substrate results in an increase in the peak area of the signals due to [2-^{13}C]GA (*28*). By contrast, we observe here that the peak area of the signal due to the C-2 protons of [2-^{13}C]GA (initially present as 0.8% of total GA) decreases during the reaction of [1-^{13}C]GA for 78 h in the presence of 240 μM K12G mutant TIM in D_2O. However, during this time, there is a small increase in the ratio of the peak areas of the signals due to the C-2 protons of [2-^{13}C]GA and [1-^{13}C]GA from 0.008 to 0.010, but no change in the ratio (0.009) of the peak areas of the signals due to the C-2 protons of [1,2-di-^{13}C]GA and [1-^{13}C]GA. These changes in relative peak areas are consistent with essentially equal velocities of conversion of the three starting isotopomers to their corresponding C-2 doubly deuteriated analogues, for which there are no ^{1}H NMR signals in the C-2 region, along with a very slow enzyme-catalyzed isomerization of [1-^{13}C]GA to give [2-^{13}C]GA. These data are consistent with conversion of $\leq$0.2% of the [1-^{13}C]GA to [2-^{13}C]GA that accompanies the much faster conversion of 20% of the [1-^{13}C]GA to [1-^{13}C,2,2-di-^{2}H]GA during this 78 h reaction. Therefore, the fractional yield of [2-^{13}C]GA [$\leq$0.006 (Table 2)] from the K12G TIM-catalyzed isomerization of [1-^{13}C]GA is estimated to be at least 100-fold lower than the fractional yield of [1-^{13}C,2,2-di-^{2}H]GA (0.56).

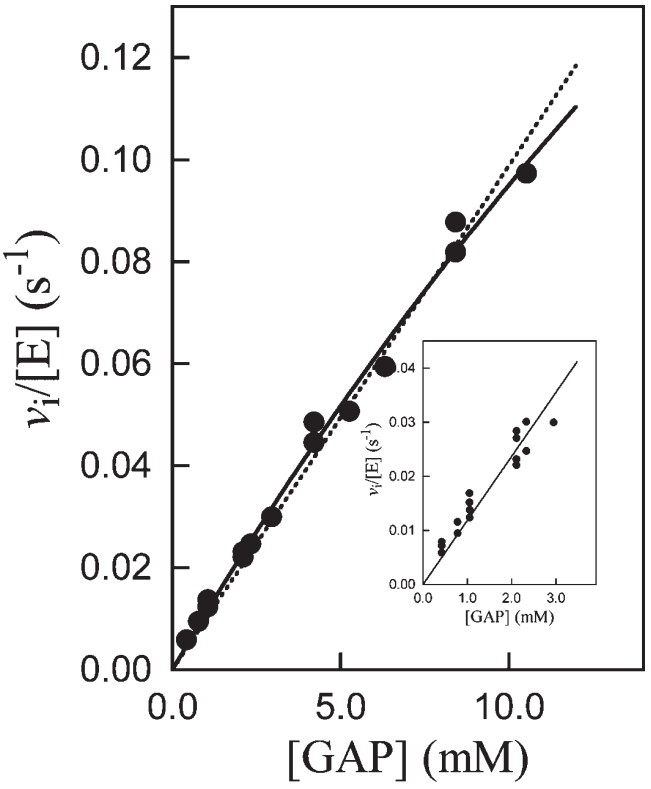

FIGURE 4: Michaelis−Menten plot of initial velocity data for the isomerization of GAP catalyzed by K12G TIM at pH 7.5 (30 mM TEA), 25 °C, and an ionic strength of 0.10 (NaCl). The solid line is the fit of the data to the Michaelis−Menten equation, and the dashed line is the linear relationship for the case in which [GAP] ≪ K_m. The inset shows the linear correlation of the data for ≤3 mM GAP, the slope of which gives a k_{cat}/K_m of 12 M^{-1} s^{-1}.

Table 2 also gives the fractional yields of the identifiable products of the K12G TIM-catalyzed reactions of [1-^{13}C]GA in the presence of 100 mM $EtND_3^+$ or 50 mM $EtND_3^+$ and 10 mM phosphite dianion. These yields were calculated from the normalized peak areas of the signals due to these products using eq 6. In all cases, the sum of the fractional yields of the products of these slow reactions of [1-^{13}C]GA is well under 100% (*28*). No attempt was made to identify the other pathways for the slow reactions of [1-^{13}C]GA in the presence of K12G TIM.

Kinetic Parameters and pH−Rate Profile for Isomerization of GAP by K12G TIM. Figure 4 shows the Michaelis−Menten plot for the isomerization of GAP catalyzed by K12G mutant yeast TIM at pH 7.5 (30 mM TEA), 25 °C, and an ionic strength of 0.10 (NaCl). The solid line shows the nonlinear least-squares fit of these data to the Michaelis−Menten equation which gave a k_{cat} of 0.6 ± 0.2 s^{-1} and a K_m of 50 ± 20 mM (Table 3); the dashed line is the linear relationship for the case in which [GAP] ≪ K_m. Table 3 also gives the much more reliable value of k_{cat}/K_m (12 ± 0.4 M^{-1} s^{-1}) that was determined as the slope of the linear correlation of the data at ≤3 mM GAP (Figure 4, inset).

Figure 5 shows the dependence of the apparent second-order rate constant $(k_{cat}/K_m)_{app}$ for K12G TIM-catalyzed isomerization of GAP (determined as the slopes of plots of v_i/[E] vs [GAP]) on the concentration of 2-phosphoglycolate (PGA) at pH 7.5, 25 °C, and an ionic strength of 0.10 (NaCl). The K_i value of 1.1 mM (Table 3) was determined from the nonlinear least-squares fit of these data to eq 7 with a k_{cat}/K_m of 12 M^{-1} s^{-1} in the absence of PGA.

$$(k_{cat}/K_m)_{app} = \frac{k_{cat}/K_m}{1 + [PGA]/K_i} \quad (7)$$

Figure 6 shows pH−rate profiles of the observed second-order rate constants $(k_{cat}/K_m)_{obs}$ for the isomerization of GAP catalyzed by wild-type TIM from chicken muscle [data of Plaut and Knowles (*35*)] and by K12G mutant yeast TIM (data from this work). The literature data for wild-type TIM were fit to eq 8, derived for Scheme 3, using a $(k_{cat}/K_m)^*$ of 0 and a pK_{SH} of 6.0 for the ionization of the phosphodianion group of GAP and a pK_{EH} of 9.2 for the ionization of an essential residue at TIM (*35*). The solid and dashed lines through the data for K12G yeast TIM compare the fit obtained using a k_{cat}/K_m of 12 M^{-1} s^{-1} (Table 3), a pK_{SH} of 6.0, a pK_{EH} of 9.2, and a $(k_{cat}/K_m)^*$ of 0 (solid line) with that using a $(k_{cat}/K_m)^*$ of 1.1 M^{-1} s^{-1} (dashed line) that was obtained from least-squares analysis that included $(k_{cat}/K_m)^*$ as an additional parameter.

$$(k_{cat}/K_m)_{obs} = \left[\frac{[H^+]}{(K_{EH} + [H^+])(K_{SH} + [H^+])}\right]\left[\left(\frac{k_{cat}}{K_m}\right)K_{SH} + \left(\frac{k_{cat}}{K_m}\right)^*[H^+]\right] \quad (8)$$

Scheme 3

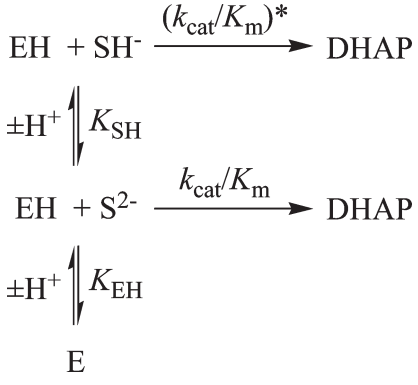

DISCUSSION

The X-ray crystal structure of yeast TIM shows that the cationic side chain of Lys-12 runs along the enzyme surface (*7*). Closure of phosphate gripper loop 6 over the substrate sequesters the carbon acid fragment from interaction with solvent, but the tip of the substrate phosphodianion group lies at the protein surface where it forms a solvent-separated ion pair with the cationic side chain of Lys-12 (*7*). X-ray crystallographic analysis of K12M/G15A TIM crystallized in the presence of the enediol(ate) intermediate analogue 2-phosphoglycolohydroxamate (PGH) revealed no bound ligand and showed that the structure of this enzyme was nearly identical to that of unliganded wild-type TIM (*22*). We therefore do not expect that the K12G mutation will result in a large change in protein structure, but it should leave a small water-filled cleft at the protein surface.

We report here a second-order rate constant k_{cat}/K_m of 12 M^{-1} s^{-1} for isomerization of GAP catalyzed by K12G mutant yeast TIM at pH 7.5, 25 °C, and an ionic strength of 0.10 (Table 3). In a previous study of the K12M mutant, the apparent k_{cat}/K_m value of 30 M^{-1} s^{-1} was attributed to the presence of ~0.0005% contaminating wild-type TIM in the mutant enzyme

Table 3: Kinetic Parameters for Isomerization of GAP by Wild-Type and K12G Mutant Yeast Triosephosphate Isomerase[a]

yeast TIM	k_{cat}[b] (s^{-1})	K_m[b] (mM)	k_{cat}/K_m (M^{-1} s^{-1})	K_i for PGA (mM)
wild type	7300 ± 400	1.1 ± 0.2	6.6×10^{6}[c]	0.019 ± 0.004[d]
K12G	0.6 ± 0.2	50 ± 20	12 ± 0.4[e]	1.1 ± 0.2[f]
effect[g]	1.2×10^{4}	50	5.5×10^{5}	60
$\Delta\Delta G$ or $\Delta\Delta G^{\ddagger}$ (kcal/mol)	5.6	2.3	7.8	2.4

[a]At pH 7.5 (30 mM TEA), 25 °C, and an ionic strength of 0.10 (NaCl). Quoted errors are standard errors obtained from least-squares analysis. [b]Determined from the fit of initial velocity data to the Michaelis−Menten equation. [c]Calculated as the ratio of the values of k_{cat} and K_m. [d]Determined by global nonlinear least-squares analysis of initial velocity data in the presence of 0, 21, and 130 μM PGA. [e]Determined as the slope of the plot of v_i/[E] vs [GAP] at ≤3 mM GAP (Figure 4, inset). [f]Determined from the nonlinear least-squares fit of the data in Figure 5 to eq 7. [g]Effect of the K12G mutation on the kinetic parameter.

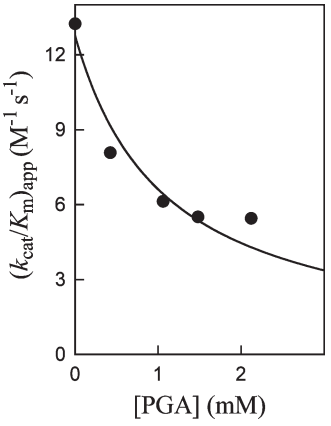

FIGURE 5: Dependence of the apparent second-order rate constant $(k_{cat}/K_m)_{app}$ for the isomerization of GAP catalyzed by K12G mutant yeast TIM on the concentration of 2-phosphoglycolate at pH 7.5 (30 mM TEA), 25 °C, and an ionic strength of 0.10 (NaCl).

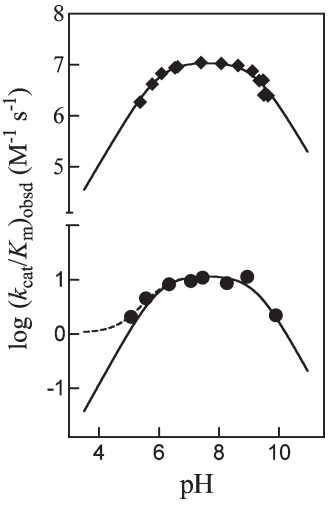

FIGURE 6: pH dependence of the observed second-order rate constant $(k_{cat}/K_m)_{obs}$ for the isomerization of GAP catalyzed by wild-type and K12G TIM. (◆) Data of Plaut and Knowles (*35*) for wild-type TIM from chicken muscle at 30 °C. The solid line shows the fit of the data to eq 8 with a $(k_{cat}/K_m)^*$ of 0. (●) Data from this work for K12G mutant yeast TIM at 25 °C. The solid and dashed lines compare the nonlinear least-squares fits of these data to eq 8 using $(k_{cat}/K_m)^*$ values of 0 and 1.1 M^{-1} s^{-1}, respectively, for turnover of GAP monoanion (Scheme 3).

preparation (*21*). By comparison, the lowered affinity of K12G TIM for GAP and PGA determined here (Table 3) shows that the observed activity of the K12G mutant cannot be due to a contaminating wild-type TIM activity. Table 3 also reports the kinetic parameters for turnover of GAP by wild-type yeast TIM determined in this work, which are in good agreement with the previously published literature values (*36*).

In an earlier study of K12M TIM, this mutant was thought to have a very weak affinity for phosphodianion ligands. The K_i value of 1.1 mM determined here for inhibition of K12G TIM by PGA at pH 7.5 (Figure 5 and Table 3) shows that the K12G mutant forms a moderately stable complex with this inhibitor trianion. However, it is more difficult to evaluate the stability of the complex of K12G TIM with GAP. The slight curvature in the Michaelis−Menten plot of v_i/[E] versus [GAP] (Figure 4) is consistent with a K_m of 50 ± 20 mM, but these data also show a reasonable fit to a linear equation. We note that (1) if the K12G mutation results in a similar 60-fold increase in the dissociation constants for both PGA and GAP, then the value of K_m for GAP would be ca. 60 mM which is close to the K_m of ≈50 mM obtained from the data in Figure 4 and (2) the effect of the K12G mutation on the affinity of the enzyme for GAP should not be any larger than the effect on its affinity for PGA, because the additional negative charge at PGA will tend to strengthen, not weaken, the interaction of the ligand with the cationic side chain of Lys-12 of the wild-type enzyme. Therefore, we conclude that K12G TIM has a weak affinity for GAP with a K_m of 50−60 mM.

K12G TIM-Catalyzed Reaction of GAP in D_2O. We reported previously that the reaction of GAP catalyzed by wild-type rabbit or chicken muscle TIM in D_2O, monitored for 2−5 h (*32*), results in the formation of the three products of the enzyme-catalyzed reaction along with substantial formation of methylglyoxal from the competing nonenzymatic elimination reaction (Scheme 2) (*14*). We observe here that the K12G mutation in yeast TIM results in a large increase in the velocity of formation of methylglyoxal over that predicted for the competing nonenzymatic elimination reaction (Table 1). This shows that K12G TIM also catalyzes the elimination reaction of GAP to give methylglyoxal (Scheme 4). Table 1 reports the normalized fractional yields f_E of the products of the enzymatic reaction of GAP catalyzed by 85 and 12 μM K12G TIM in D_2O at pD 7.9. These yields were calculated using eq 9, where $(f_{MG})_E$ is the fractional yield of methylglyoxal from the enzymatic reaction that was calculated from the total fractional yield of methylglyoxal $(f_{MG})_{tot}$ as described in Results.

$$f_E = \frac{(f_P)_o}{(f_{DHAP})_o + (f_{d\text{-}DHAP})_o + (f_{d\text{-}GAP})_o + (f_{MG})_E} \quad (9)$$

$$(f_E)_{PT} = \frac{(f_P)_o}{(f_{DHAP})_o + (f_{d\text{-}DHAP})_o + (f_{d\text{-}GAP})_o} \quad (10)$$

A rate constant ratio k_{PT}/k_{elim} of ≈1×10^6 was estimated for partitioning of the enzyme-bound enediol(ate) phosphate

Scheme 4

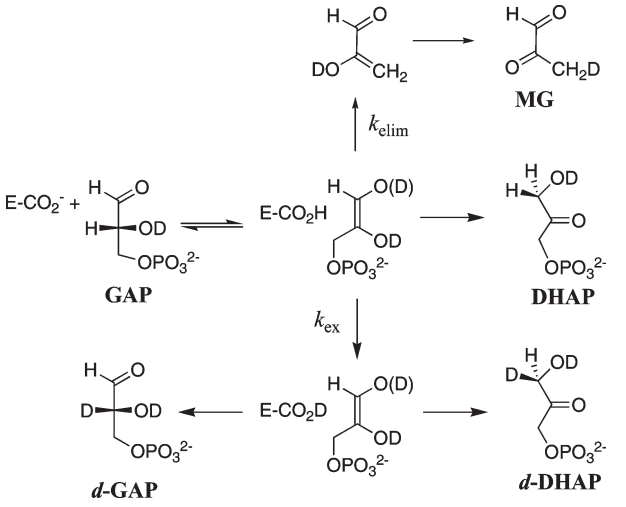

intermediate of the wild-type TIM-catalyzed reaction between protonation at carbon and elimination of inorganic phosphate (*37*). This is much larger than the k_{PT}/k_{elim} of 6.5 for partitioning of the same enediol(ate) phosphate between proton transfer at carbon and elimination of phosphate within a loose complex with a small tertiary ammonium cation in solution (*14*). These observations show that interactions with wild-type TIM strongly stabilize the bound enediol(ate) phosphate intermediate toward elimination of inorganic phosphate (*37*, *38*). The absence of the alkylammonium side chain of Lys-12 of K12G mutant yeast TIM results in a dramatic change in the ratio of the yields of the products of proton transfer and elimination (Scheme 4), from a k_{PT}/k_{elim} of $\approx 1 \times 10^6$ (*37*) to a value of 4.5 (0.81/0.18) (Table 1). This dramatic change in the partitioning of the enediol(ate) phosphate intermediate shows that interaction of the cationic side chain of Lys-12 with the bound enediol(ate) phosphate strongly protects this species from elimination of inorganic phosphate. Good yields of methylglyoxal are also observed from the reactions of GAP and DHAP catalyzed by a loop deletion mutant of TIM (*38*), because interactions between the enediol(ate) phosphate and the flexible loop (loop 6) of TIM play a vital role in preventing breakdown of the intermediate with the loss of inorganic phosphate.

Table 1 also reports the normalized fractional yields $(f_E)_{PT}$ of the three products of the transfer of a proton to the enzyme-bound enediol(ate) intermediate of the reactions of GAP catalyzed by wild-type TIM from rabbit or chicken muscle (*32*) and K12G mutant yeast TIM (this work, calculated using eq 10). These data show that the K12G mutation causes the yield of DHAP formed by intramolecular transfer of hydrogen from substrate GAP to decrease from 49% for the wild-type enzyme to 33% for the K12G mutant. There is good evidence that the H-labeled carboxylic acid side chain of Glu-165 of the TIM·enediol(ate) complex is sequestered from bulk solvent D_2O and that this residue undergoes exchange with a small pool of similarly sequestered hydrons followed by the transfer of a proton to the enediol(ate) to form *d*-GAP and *d*-DHAP (Scheme 4) (*39*, *40*). Therefore, the decrease in the yield of the product of intramolecular transfer of hydrogen is nominally consistent with the conclusion that the K12G mutation increases the accessibility of the active site to the bulk solvent. The K12G mutation also results in an increase in the ratio of the yields of *d*-GAP and *d*-DHAP, from 0.7 for wild-type TIM to 1.3 for the K12G mutant. However, these small effects are difficult to rationalize in comparison with the very large 6×10^5-fold effect of the K12G mutation on k_{cat}/K_m for isomerization of GAP (Table 3).

We conclude that Lys-12 plays an important role in stabilizing both the transition state for deprotonation of GAP and of the bound enediol(ate) intermediate toward elimination of phosphate dianion. However, it plays a much less important role in controlling the partitioning of the enediol(ate) intermediate in D_2O among DHAP, *d*-GAP, and *d*-DHAP.

K12G TIM-Catalyzed Reaction of [1-^{13}C]GA in D_2O. The large difference between the k_{cat}/K_m for the isomerization of GAP (1.0×10^8 M^{-1} s^{-1})[3] and that for the deprotonation of glycolaldehyde ($\sim$0.10 M^{-1} s^{-1})[4] by wild-type chicken muscle TIM shows that interactions between the substrate phosphodianion and TIM provide an $\sim$12 kcal/mol stabilization (intrinsic phosphate binding energy) of the transition state for proton transfer from GAP (*12*, *16*). Truncation of GAP to give the neutral substrate glycolaldehyde eliminates transition state stabilization resulting from interactions with the phosphodianion group. Therefore, the observation of a large effect of the K12G mutation on the rate constant for deprotonation of glycolaldehyde would provide direct evidence of stabilizing interactions between the excised cationic side chain of Lys-12 and the carbon acid substrate piece. This two-part substrate approach was used to probe the interactions of amino acid side chains with the phosphodianion and nucleoside portions of the substrate in the decarboxylation of orotidine 5′-monophosphate catalyzed by orotidine 5′-monophosphate decarboxylase (*41*).

We reported previously that the reaction of [1-^{13}C]GA catalyzed by wild-type chicken muscle TIM gives an $\sim$50% combined yield of isomerization product [2-^{13}C]GA, the product of isomerization with deuterium exchange ([2-^{13}C,2-^{2}H]GA), and the product of deuterium exchange ([1-^{13}C,2-^{2}H]GA) resulting from the "specific" reactions of [1-^{13}C]GA at the enzyme active site (*28*) (Scheme 5). By contrast, the only clearly detectable product of the reaction of [1-^{13}C]GA catalyzed by K12G mutant yeast TIM is the dideuteriated isotopomer [1-^{13}C,2,2-di-^{2}H]GA which is formed in $\sim$56% yield (Table 2). This isotopomer was also observed as a minor product ($\sim$20% yield) of the wild-type chicken muscle TIM-catalyzed reaction, where it was proposed to form by a "nonspecific" protein-catalyzed reaction that occurs outside the enzyme active site (*28*).

Scheme 5

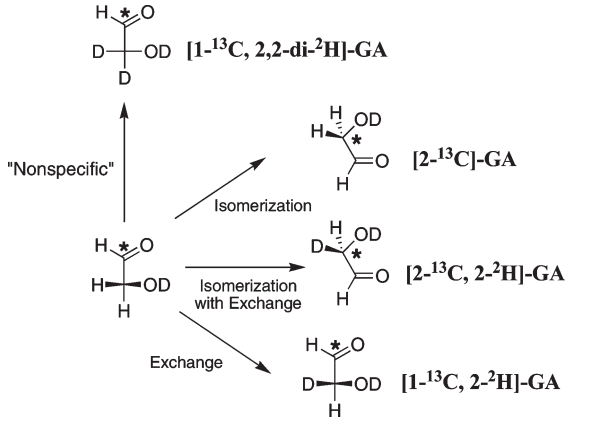

[3]Values for k_{cat} of 2300 s^{-1} and K_m of 0.45 mM for isomerization of GAP by chicken muscle TIM at pH 7.5 and 25 °C were reported in our earlier work (*28*). GAP exists as 95% hydrate and 5% free carbonyl (the reactive form) in D_2O at pD 7.9, 25 °C, and an ionic strength of 0.10 (NaCl) (*32*).

The second-order rate constant (k_{cat}/K_m) for the nonspecific K12G TIM-catalyzed reaction of [1-^{13}C]GA to give [1-^{13}C,2,2-di-^{2}H]GA that occurs outside the active site can be calculated as (0.11 M^{-1} s^{-1})(0.56) = 0.062 M^{-1} s^{-1}, where 0.11 M^{-1} s^{-1} is the observed second-order rate constant for the K12G TIM-catalyzed disappearance of [1-^{13}C]GA and 0.56 is the fractional yield of [1-^{13}C,2,2-di-^{2}H]GA (Table 2). This rate constant is at least 90-fold larger than the $(k_{cat}/K_m)_{iso}$ of $\leq 7 \times 10^{-4}$ M^{-1} s^{-1} for the isomerization of [1-^{13}C]GA at the active site to give [2-^{13}C]GA (Table 2). The corresponding second-order rate constant for the isomerization of [1-^{13}C]GA catalyzed by wild-type chicken muscle TIM can be calculated from data in our previous work as $(k_{cat}/K_m)_{iso} = 9.5 \times 10^{-3}$ M^{-1} s^{-1} (*28*).[5] Therefore, the K12G mutation results in an at least 14-fold decrease in $(k_{cat}/K_m)_{iso}$ for the isomerization of [1-^{13}C]GA. This provides direct evidence that the cationic side chain of Lys-12 stabilizes the transition state for the transfer of a proton from glycolaldehyde by interaction with the carbon acid substrate piece. It is reasonable to conclude that this side chain also acts similarly to stabilize the transition sate for isomerization of GAP by interaction with both the nonreacting phosphodianion and the reacting carbon acid fragments of the whole substrate.

Phosphite dianion strongly activates wild-type rabbit and chicken muscle TIM toward the isomerization of glycolaldehyde (*28*, *30*), and we have also found that alkylammonium cations strongly activate K12G mutant yeast TIM toward the isomerization of GAP (*42*). We therefore examined the K12G TIM-catalyzed reaction of [1-^{13}C]GA in D_2O in the presence of 100 mM $EtND_3^+$ or 50 mM $EtND_3^+$ and 10 mM phosphite dianion (Table 2). These reagents result in small increases in the observed second-order rate constant $(k_{cat}/K_m)_{obs}$ for the disappearance of [1-^{13}C]GA (Table 2). However, these increases do not result from catalysis of isomerization at the enzyme active site because there is no detectable formation of the isomerization product [2-^{13}C]GA (Table 2). No attempt was made to characterize the additional products of these slow reactions because the products do not appear to be formed at the active site of TIM. We reach the following conclusions. (1) Interactions between the phosphite dianion activator and the cationic side chain of Lys-12 are essential for the observation of phosphite activation of the TIM-catalyzed deprotonation of GA (*30*). (2) Interactions between the phosphodianion group of GAP and exogenous ammonium cations are essential for the observation of rescue of the activity of K12G mutant TIM by these cations (*42*). However, K12G mutant TIM shows no detectable activity for isomerization of [1-^{13}C]GA in the presence of $EtND_3^+$ and phosphite dianion, presumably because these ions show a weak affinity for binding to the mutant enzyme.

pH−Rate Profile for Isomerization of GAP by K12G Mutant Yeast TIM. Figure 6 shows the pH−rate profiles for k_{cat}/K_m for the isomerization of GAP catalyzed by wild-type chicken muscle TIM (data from ref *35*) and K12G mutant yeast TIM (data from this work). The solid lines show the fits of the data to eq 8 with a $(k_{cat}/K_m)^*$ of 0. The dashed line for K12G TIM shows that the inclusion of the $(k_{cat}/K_m)^*$ of 1.1 M^{-1} s^{-1} for the turnover of GAP monoanion results in a small improvement in the fit of the experimental data to eq 8 (see Results). This suggests that K12G TIM exhibits an only ~10-fold selectivity for catalysis of the isomerization of GAP dianion [(k_{cat}/K_m) = 12 M^{-1} s^{-1} (Table 3)] over GAP monoanion [$(k_{cat}/K_m)^*$ = 1.1 M^{-1} s^{-1}].

The downward break centered at pH 9.2 for wild-type TIM cannot be due to deprotonation of the cationic side chain of Lys-12 because the same break is observed in the profile for K12G TIM (Figure 6).[6] This demonstrates that $pK_a > 9.2$ for the cationic side chain of Lys-12, which is consistent with the salt bridge with the carboxylate side chain of Glu-97 observed for TIM·PGA and TIM·PGH complexes (*10*, *17*, *43*). It also suggests that there is a large distance between the side chains of Lys-12 and this second critical residue.

Specificity in Transition State Binding. The K12G mutation in yeast TIM results in a 5.5×10^5-fold decrease in k_{cat}/K_m for the isomerization of GAP (Table 3), corresponding to a 7.8 kcal/mol stabilization of the transition state by the cationic side chain of Lys-12. This effect can be partitioned into an ~50-fold effect on K_m ($\Delta\Delta G$ = 2.3 kcal/mol) and a much larger ~12000-fold effect on k_{cat} for the isomerization of the bound substrate [$\Delta\Delta G^{\ddagger}$ = 5.6 kcal/mol (Table 3)]. The effect of the mutation on K_m can be directly attributed to the loss of ground state electrostatic interactions between the substrate phosphodianion group and the cationic side chain of Lys-12. More importantly, the large effect on k_{cat} shows that there is a significant strengthening of the interactions between the ligand and the alkylammonium side chain of Lys-12 on moving from the ground state Michaelis complex to the transition state for carbon deprotonation. The most striking structural change on moving from the Michaelis complex to the enediol(ate)-like transition state for deprotonation of GAP is the change in formal charge at the substrate carbonyl oxygen, from 0 to −1, and the change in the total charge at bound ligand, from −2 to −3. This increase in negative charge is expected to result in an increase in the strength of the stabilizing electrostatic interactions between the alkylammonium side chain of Lys-12 and the altered substrate in the transition state (*44*).

The K12G mutation also results in an at least 14-fold decrease in $(k_{cat}/K_m)_{iso}$ for the isomerization of bound glycolaldehyde (vide infra), which shows that the cationic side chain of Lys-12 acts to stabilize the transition state for the transfer of a proton from a neutral substrate piece that lacks a phosphodianion group. This provides evidence of a significant stabilizing interaction between the cationic side chain of Lys-12 and the developing negative charge on the sugar substrate piece in an enediol(ate)-like transition state. It is in accord with computational studies that pointed to the dominant role of Lys-12 in the stabilization of the transition state for formation of an enediolate intermediate by carbon deprotonation of the whole substrate DHAP or GAP (*44*, *45*).

The role of Lys-12 in catalysis of isomerization has also been inferred from an inspection of the X-ray crystal structure of yeast TIM in a complex with DHAP (Figure 7) (*7*). The alkylammonium side chain of Lys-12 lies roughly equidistant from the phosphodianion and carbonyl groups of bound DHAP and is expected to interact with both centers. This side chain likely does not form a hydrogen bond with the phosphate dianion in the

[4]Calculated using a $(k_{cat}/K_m)_{obs}$ of 0.19 M^{-1} s^{-1} for the enzyme-catalyzed disappearance of glycolaldehyde and the observation that 50% of the products of this reaction result from deprotonation of glycolaldehyde within the active site (*28*).

[5]Calculated using a $(k_{cat}/K_m)_{obs}$ of 0.19 M^{-1} s^{-1} for the enzyme-catalyzed disappearance of glycolaldehyde and the observation that the isomerization product [2-^{13}C]GA is formed in a yield of 5% (*28*).

[6]The similarity of the kinetic parameters for wild-type TIM from chicken muscle (*35*) and yeast (Table 3 and ref *36*) at pH 7.5 suggests that the appearance of the pH−rate profiles for these enzymes should also be similar.

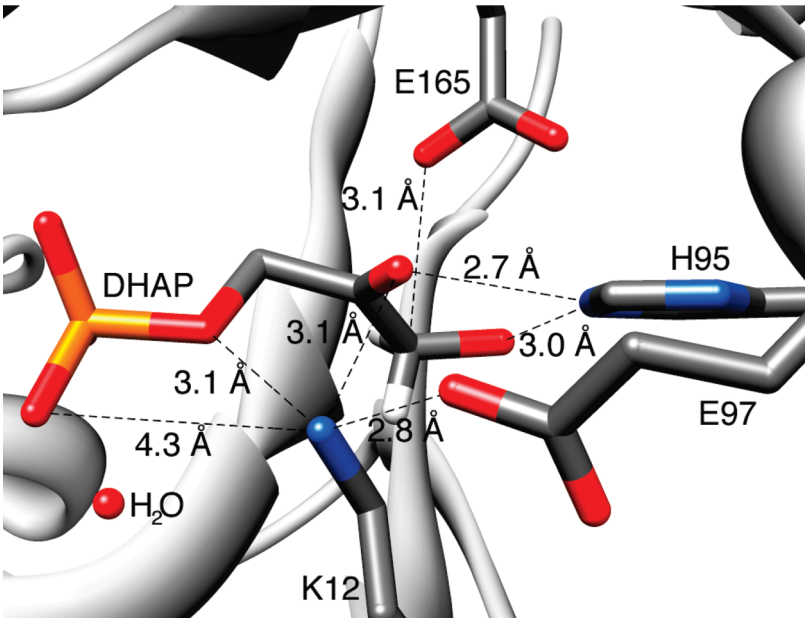

FIGURE 7: Structure of the active site of TIM, taken from the X-ray crystal structure of McDermott and co-workers (Protein Data Bank entry 1NEY) (*7*), showing the distances between the ammonium nitrogen of Lys-12 and the functional groups of bound substrate DHAP.

ground state Michaelis complex because the X-ray crystal structure reveals the presence of a water molecule between the cationic side chain of Lys-12 and the phosphodianion group of DHAP, which attenuates the electrostatic interaction (Figure 7) (*7*). This interaction might be strengthened by a shift in the position of the water to allow for greater proximity between the interacting charges at the transition state for proton transfer. However, we have no evidence to support this proposal, and we note that a bridging water molecule in this position is also observed for complexes between TIM and the intermediate analogues PGH (*43*) and PGA (*10*).

The stretching frequency for the C-2 carbonyl group of DHAP bound to the H95Q and H95N mutants of yeast TIM lies between 1732 and 1742 cm^{-1} (*46*), which is similar to the carbonyl stretching frequency of 1732 cm^{-1} for DHAP in water (*47*). This suggests that there is no additional polarization of the carbonyl π-bond of enzyme-bound DHAP due to a hydrogen bonding interaction with Lys-12 (*21*). Although there is no crystal structure for the complex between TIM and GAP, the large effect of the K12G mutation on k_{cat} for the isomerization of GAP (Table 3) provides strong evidence that the cationic side chain of Lys-12 stabilizes negative charge that develops on O-1 at the transition state for deprotonation of GAP.

Charged Enediolate or Neutral Enediol Intermediate? Studies of the nonenzymatic deprotonation of GAP in water show that direct Brønsted base-catalyzed deprotonation of the substrate to form a negatively charged enediolate intermediate is favored energetically over any competing Brønsted acid-catalyzed pathway to form the enediol (*14*). This is because the enolate oxygen of the enediolate intermediate is relatively weakly basic [$pK_a \approx 11$ for the enol (*14*, *48*)], so that there is no significant advantage to concerted catalysis by relatively weak Brønsted acids (*49*). Brønsted general acid catalysis of the deprotonation of enzyme-bound GAP to form an enediol intermediate would be favored if the transfer of a proton from the enzyme to the enediolate were strongly favorable (*50*).

We suggest that there is a strong catalytic imperative to the avoidance of the full transfer of a proton to the enediolate oxyanion which dictates the use of a neutral imidazole side chain of His-95 (*25*), rather than the more acidic imidazolium cation, as the catalytic electrophile at TIM. Full proton transfer to the enediolate oxyanion would eliminate the large stabilizing electrostatic interaction with the cationic side chain of Lys-12. However, partial proton transfer from the neutral imidazole of His-95 to the oxyanion allows for effective transition state stabilization by hydrogen bonding (*46*), while at the same time maintaining the critical stabilizing electrostatic interaction with the cationic side chain of Lys-12.

It is not obvious that enolate anions, whose formation from neutral molecules is intrinsically more difficult in solvents with low dielectric constants than in water, should in fact be formed more easily at the nonpolar active sites of protein catalysts (*51*−*55*) than in aqueous solution. However, zwitterions are strongly stabilized by their transfer from aqueous solution to organic solvents (*56*−*58*), and the formation of the effectively intramolecular (*59*, *60*) ion pairs between enzyme catalysts and immobilized bound substrates will be favored entropically over the bimolecular formation of ion pairs between small molecules in solution. Others have noted that enzyme active sites provide a highly organized environment for chemical reactions (*51*, *61*, *62*), where appropriately placed amino acid side chains act to stabilize bound ions with opposite charges.

REFERENCES

1. Knowles, J. R., and Albery, W. J. (1977) Perfection in enzyme catalysis: The energetics of triosephosphate isomerase. *Acc. Chem. Res. 10*, 105–111.
2. Rieder, S. V., and Rose, I. A. (1959) Mechanism of the triose phosphate isomerase reaction. *J. Biol. Chem. 234*, 1007–1010.
3. Shonk, C. E., and Boxer, G. E. (1964) Enzyme patterns in human tissues. I. Methods for the determination of glycolytic enzymes. *Cancer Res. 24*, 709–721.
4. Gerlt, J. A., and Gassman, P. G. (1993) Understanding the rates of certain enzyme-catalyzed reactions: Proton abstraction from carbon acids, acyl transfer reactions, and displacement reactions of phosphodiesters. *Biochemistry 32*, 11943–11952.
5. Richard, J. P., and Amyes, T. L. (2001) Proton transfer at carbon. *Curr. Opin. Chem. Biol. 5*, 626–633.

6. Amyes, T. L., and Richard, J. P. (2007) Proton Transfer to and from carbon in model systems. In Hydrogen-Transfer Reactions, Volume 3. Biological Aspects I-II (Hynes, J. T., Klinman, J. P., Limbach, H.-H., and Schowen, R. L., Eds.) pp 949−973, Wiley-VCH, Weinheim, Germany.
7. Jogl, G., Rozovsky, S., McDermott, A. E., and Tong, L. (2003) Optimal alignment for enzymatic proton transfer: Structure of the Michaelis complex of triosephosphate isomerase at 1.2-Å resolution. *Proc. Natl. Acad. Sci. U.S.A. 100*, 50–55.
8. Xiang, J., Sun, J., and Sampson, N. S. (2001) The importance of hinge sequence for loop function and catalytic activity in the reaction catalyzed by triosephosphate isomerase. *J. Mol. Biol. 307*, 1103–1112.
9. Xiang, J., Jung, J.-y., and Sampson, N. S. (2004) Entropy effects on protein hinges: The reaction catalyzed by triosephosphate isomerase. *Biochemistry 43*, 11436–11445.
10. Kursula, I., and Wierenga, R. K. (2003) Crystal structure of triosephosphate isomerase complexed with 2-phosphoglycolate at 0.83-Å resolution. *J. Biol. Chem. 278*, 9544–9551.
11. Blacklow, S. C., Raines, R. T., Lim, W. A., Zamore, P. D., and Knowles, J. R. (1988) Triosephosphate isomerase catalysis is diffusion controlled. *Biochemistry 27*, 1158–1165.
12. Amyes, T. L., O'Donoghue, A. C., and Richard, J. P. (2001) Contribution of phosphate intrinsic binding energy to the enzymatic rate acceleration for triosephosphate isomerase. *J. Am. Chem. Soc. 123*, 11325–11326.
13. Morrow, J. R., Amyes, T. L., and Richard, J. P. (2008) Phosphate binding energy and catalysis by small and large molecules. *Acc. Chem. Res. 41*, 539–548.
14. Richard, J. P. (1984) Acid-base catalysis of the elimination and isomerization reactions of triose phosphates. *J. Am. Chem. Soc. 106*, 4926–4936.
15. Amyes, T. L., Richard, J. P., and Tait, J. J. (2005) Activation of orotidine 5′-monophosphate decarboxylase by phosphite dianion: The whole substrate is the sum of two parts. *J. Am. Chem. Soc. 127*, 15708–15709.
16. Tsang, W.-Y., Amyes, T. L., and Richard, J. P. (2008) A substrate in pieces: Allosteric activation of glycerol 3-phosphate dehydrogenase (NAD^+) by phosphite dianion. *Biochemistry 47*, 4575–4582.
17. Lolis, E., and Petsko, G. A. (1990) Crystallographic analysis of the complex between triosephosphate isomerase and 2-phosphoglycolate at 2.5-Å resolution: Implications for catalysis. *Biochemistry 29*, 6619–6625.
18. Knowles, J. R. (1991) To build an enzyme. *Philos. Trans. R. Soc. London, Ser. B 332*, 115–121.
19. Klotz, I. M., and Franzen, J. S. (1962) Hydrogen bonds between model peptide groups in solution. *J. Am. Chem. Soc. 84*, 3461–3466.
20. Susi, H., Timasheff, S. N., and Ard, J. S. (1964) Near infrared investigation of interamide hydrogen bonding in aqueous solution. *J. Biol. Chem. 239*, 3051–3054.
21. Lodi, P. J., Chang, L. C., Knowles, J. R., and Komives, E. A. (1994) Triosephosphate isomerase requires a positively charged active site: The role of lysine-12. *Biochemistry 33*, 2809–2814.
22. Joseph-McCarthy, D., Lolis, E., Komives, E. A., and Petsko, G. A. (1994) Crystal structure of the K12M/G15A triosephosphate isomerase double mutant and electrostatic analysis of the active site. *Biochemistry 33*, 2815–2823.
23. O'Connor, E. J., Tomita, Y., and McDermott, A. E. (1994) Synthesis of (1,2-$^{13}C_2$)-2-phosphoglycolic acid. *J. Labelled Compd. Radiopharm. 34*, 735–740.
24. Bergemeyer, H. U., Haid, E., Nelboeck-Hochstetter, M., and Pelz, O. (1972) Process for preparing open ring tetrose and triose phosphate acetals and phosphate ketals. U. S. Patent 3,662,037.
25. Lodi, P. J., and Knowles, J. R. (1991) Neutral imidazole is the electrophile in the reaction catalyzed by triosephosphate isomerase: Structural origins and catalytic implications. *Biochemistry 30*, 6948–6956.
26. Straus, D., and Gilbert, W. (1985) Chicken triosephosphate isomerase complements an *Escherichia coli* deficiency. *Proc. Natl. Acad. Sci. U.S.A. 82*, 2014–2018.
27. Sun, J., and Sampson, N. S. (1999) Understanding protein lids: Kinetic analysis of active hinge mutants in triosephosphate isomerase. *Biochemistry 38*, 11474–11481.
28. Go, M. K., Amyes, T. L., and Richard, J. P. (2009) Hydron transfer catalyzed by triosephosphate isomerase. Products of the direct and phosphite-activated isomerization of [1-^{13}C]-glycolaldehyde in D_2O. *Biochemistry 48*, 5769–5778.
29. Glasoe, P. K., and Long, F. A. (1960) Use of glass electrodes to measure acidities in deuterium oxide. *J. Phys. Chem. 64*, 188–190.
30. Amyes, T. L., and Richard, J. P. (2007) Enzymatic catalysis of proton transfer at carbon: Activation of triosephosphate isomerase by phosphite dianion. *Biochemistry 46*, 5841–5854.
31. Collins, G. C. S., and George, W. O. (1971) Nuclear magnetic resonance spectra of glycolaldehyde. *J. Chem. Soc. B,* 1352–1355.
32. O'Donoghue, A. C., Amyes, T. L., and Richard, J. P. (2005) Hydron transfer catalyzed by triosephosphate isomerase. Products of isomerization of (*R*)-glyceraldehyde 3-phosphate in D_2O. *Biochemistry 44*, 2610–2621.
33. Gasteiger, E., Gattiker, A., Hoogland, C., Ivanyi, I., Appel, R. D., and Bairoch, A. (2003) ExPASy: The proteomics server for in-depth protein knowledge and analysis. *Nucleic Acids Res. 31*, 3784–3788.
34. Gasteiger, E., Hoogland, C., Gattiker, A., Duvaud, S., Wilkins, M. R., Appel, R. D., and Bairoch, A. (2005) in Proteomics Protocols Handbook (Walker, J. M., Ed.) pp 571−607, Humana Press Inc., Totowa, NJ.
35. Plaut, B., and Knowles, J. R. (1972) pH-dependence of the triose phosphate isomerase reaction. *Biochem. J. 129*, 311–320.
36. Nickbarg, E. B., and Knowles, J. R. (1988) Triosephosphate isomerase: Energetics of the reaction catalyzed by the yeast enzyme expressed in *Escherichia coli*. *Biochemistry 27*, 5939–5947.
37. Richard, J. P. (1991) Kinetic parameters for the elimination reaction catalyzed by triosephosphate isomerase and an estimation of the reactions physiological significance. *Biochemistry 30*, 4581–4585.
38. Pompliano, D. L., Peyman, A., and Knowles, J. R. (1990) Stabilization of a reaction intermediate as a catalytic device: Definition of the functional role of the flexible loop in triosephosphate isomerase. *Biochemistry 29*, 3186–3194.
39. O'Donoghue, A. C., Amyes, T. L., and Richard, J. P. (2005) Hydron transfer catalyzed by triosephosphate isomerase. Products of isomerization of dihydroxyacetone phosphate in D_2O. *Biochemistry 44*, 2622–2631.
40. O'Donoghue, A. C., Amyes, T. L., and Richard, J. P. (2008) Slow proton transfer from the hydrogen-labelled carboxylic acid side chain (Glu-165) of triosephosphate isomerase to imidazole buffer in D_2O. *Org. Biomol. Chem. 6*, 391–396.
41. Barnett, S. A., Amyes, T. L., Wood, B. M., Gerlt, J. A., and Richard, J. P. (2008) Dissecting the Total Transition State Stabilization Provided by Amino Acid Side Chains at Orotidine 5′-Monophosphate Decarboxylase: A Two-Part Substrate Approach. *Biochemistry 47*, 7785–7787.
42. Go, M. K. (2009) Studies on enzymatic and non-enzymatic proton transfer in aqueous solutions. Ph.D. Thesis, University at Buffalo, State University of New York, Buffalo, NY.
43. Davenport, R. C., Bash, P. A., Seaton, B. A., Karplus, M., Petsko, G. A., and Ringe, D. (1991) Structure of the triosephosphate isomerase-phosphoglycolohydroxamate complex: An analog of the intermediate on the reaction pathway. *Biochemistry 30*, 5821–5826.
44. Bash, P. A., Field, M. J., Davenport, R. C., Petsko, G. A., Ringe, D., and Karplus, M. (1991) Computer simulation and analysis of the reaction pathway of triosephosphate isomerase. *Biochemistry 30*, 5826–5832.
45. Cui, Q., and Karplus, M. (2001) Triosephosphate isomerase: A theoretical comparison of alternative pathways. *J. Am. Chem. Soc. 123*, 2284–2290.
46. Komives, E. A., Chang, L. C., Lolis, E., Tilton, R. F., Petsko, G. A., and Knowles, J. R. (1991) Electrophilic catalysis in triosephosphate isomerase: The role of histidine-95. *Biochemistry 30*, 3011–3019.
47. Belasco, J. G., and Knowles, J. R. (1980) Direct observation of substrate distortion by triosephosphate isomerase using Fourier transform infrared spectroscopy. *Biochemistry 19*, 472–477.
48. Keeffe, J. R., and Kresge, A. J. (1990) Kinetics and mechanism of enolization and ketonization. In The Chemistry of Enols (Rappoport, Z., Ed.) pp 399−480, John Wiley and Sons, Chichester, U.K.
49. Jencks, W. P. (1972) Requirements for general acid-base catalysis of complex reactions. *J. Am. Chem. Soc. 94*, 4731–4732.
50. Richard, J. P. (1998) The Enhancement of Enzymatic Rate Accelerations by Brønsted Acid-Base Catalysis. *Biochemistry 37*, 4305–4309.
51. Sham, Y. Y., Muegge, I., and Warshel, A. (1998) The effect of protein relaxation on charge-charge interactions and dielectric constants of proteins. *Biophys. J. 74*, 1744–1753.
52. Simonson, T., and Brooks, C. L. (1996) Charge Screening and the Dielectric Constant of Proteins: Insights for Molecular Dynamics. *J. Am. Chem. Soc. 118*, 8452–8458.
53. Simonson, T., Carlsson, J., and Case, D. A. (2004) Proton Binding to Proteins: pK_a Calculations with Explicit and Implicit Solvent Models. *J. Am. Chem. Soc. 126*, 4167–4180.
54. Antosiewicz, J., McCammon, J. A., and Gilson, M. K. (1996) The determinants of pK_as in proteins. *Biochemistry 35*, 7819–7833.
55. Georgescu, R. E., Alexov, E. G., and Gunner, M. R. (2002) Combining conformational flexibility and continuum electrostatics for calculating pK_as in proteins. *Biophys. J. 83*, 1731–1748.

56. Richard, J. P., and Amyes, T. L. (2004) On the importance of being zwitterionic: Enzymic catalysis of decarboxylation and deprotonation of cationic carbon. *Bioorg. Chem. 32*, 354–366.
57. Rios, A., Amyes, T. L., and Richard, J. P. (2000) Formation and stability of organic zwitterions in aqueous solution: Enolates of the amino acid glycine and its derivatives. *J. Am. Chem. Soc. 122*, 9373–9385.
58. Price, W. D., Jockusch, R. A., and Williams, E. R. (1998) Binding energies of protonated betaine complexes: A probe of zwitterion structure in the gas phase. *J. Am. Chem. Soc. 120*, 3474–3484.
59. Jencks, W. P. (1975) Binding energy, specificity and enzymic catalysis: The Circe effect. *Adv. Enzymol. Relat. Areas Mol. Biol. 43*, 219–410.
60. Jencks, W. P. (1981) On the attribution and additivity of binding energies. *Proc. Natl. Acad. Sci. U.S.A. 78*, 4046–4050.
61. Warshel, A. (1998) Electrostatic origin of the catalytic power of enzymes and the role of preorganized active sites. *J. Biol. Chem. 273*, 27035–27038.
62. Cannon, W. R., and Benkovic, S. J. (1998) Solvation, Reorganization Energy, and Biological Catalysis. *J. Biol. Chem. 273*, 26257–26260.